



## A New Texture Segmentation Method with Energy-driven Parametric Active Contour Model Based on Jensen-Tsallis Divergence

M. Nouri, Y. Baleghi Damavandi\*

Department of Electrical & Computer Engineering, Babol Noshirvani University of Technology, Babol, Iran

### PAPER INFO

#### Paper history:

Received 18 December 2021

Received in revised form 18 March 2022

Accepted 28 March 2022

#### Keywords:

Co-occurrence Matrix

Parametric Active Contour Model

Jensen -Tsallis Divergence

Balloon Energy

Texture Segmentation

### ABSTRACT

Texture image segmentation plays an important role in various computer vision tasks. Active contour models are one of the most efficient and popular methods for identifying the purpose and segmentation of objects in the image. This paper presents a parametric active contour model (PACM) with a robust minimization framework based on image texture energy. First, the texture features of the original image are extracted using gray level co-occurrence matrix (GLCM). Subsequently, based on the GLCM texture features inside and outside the active contour, Jensen-Tsallis divergence of energies is calculated. The Jensen-Tsallis divergence is added to the parametric active contour using the balloon equation. The divergence is maximum at the boundary between the foreground and background of the image, which results in minimizing the active contour equation at the boundary of the target object. This global minimization energy function with texture feature can avoid the existence of local minima in the PACM models. Also, as opposed to previous models, the proposed model only requires the initial contour and is not dependent on the distance of the initial contour from the target object. In terms of segmentation accuracy and efficiency, experiments with synthetic and natural images demonstrate that the proposed approach obtains more satisfactory results than the previous state-of-the-art methods.

doi: 10.5829/ije.2022.35.07a.05

## 1. INTRODUCTION

Segmentation is one of the prime parts of image processing. Boundary detection plays an important role in machine vision applications, such as control of urban transportation systems [1], video surveillance [2], medical diagnosis [3-6], identifying military targets [7], plants monitoring [8-10] and object tracking [11-15]. One of the important areas in image segmentation is the division of an image into areas with different textural features [16]. This has been the focus of researchers for a long time. So far, no identified method has been proposed for segmenting images with non-uniform textures that can segment all textures. In general, the quality of textural image segmentation depends on the performance of texture description algorithms as well as the choice of segmentation method [17]. Many methods for segmenting images have been introduced, including region growth, division, integration, neural networks (ANN), active contour (ACM) models, etc [18]. Active contour models are recognized as one of the most

successful methods for segmenting images [19, 20]. Active contour models have many advantages over other algorithms [21, 22]. First, active contour models show the coordinates of boundary pixels well. Second, it is possible to add image region information to the active contour to improve the quality of texture segmentation. Third, the resulting contour is a closed and regular contour that is very suitable for applications such as segmentation, detection, and analysis of an image [23].

Based on basic equations for active contours, the models of active contours can be divided into geometric [24] and parametric [25] categories. The basic equations of active contour models consist of two parts: internal energy, and external energy. Internal energy is not dependent on image and is simply a mathematical definition of a discrete contour [26]. External energy is an equation that is derived from the content of the image and helps to converge the active contour to the object boundary [25]. Researchers have so far been able to define external energy equations in edge-based (traditional) and region-based methods [18]. Edge-based

\*Corresponding Author Institutional Email: [y.baleghi@nit.ac.ir](mailto:y.baleghi@nit.ac.ir)  
(Y. Baleghi Damavandi)

active contours use an edge detection algorithm to stop the active contour from moving at the target object boundary [16]. Therefore, edge-based methods will be incapable of dealing with images with weak borders. To overcome this problem, researchers have tried to use region information to improve the performance of the active contour [27-29]. Region-based active contours are stronger when facing low-contrast images (weak edges) and are also less sensitive to the position of the starting points of the active contour [23].

Therefore, to overcome this problem in low-edge images, Ivins and Porri [30] and Schaub and Smith [31] introduced different models of color active contour. In turn, Hamarneh et al. [32] introduced a type of color active contour in which inflatable energy is used to guide the contour towards the target. This energy uses normalized RGB color space or HSV color space to produce color pressure energy. This model used an active contour in medical images to segment oral lesions. In this method, the energy of color pressure is added to the energy function of the parametric active contour model. The energy is directed to the target object with a specific color using the new energy function of the active contour. The technique was used in medical image segmentation and mobile image lighting. This method makes it possible to segment targets that have weak borders. In this method, the target and the background should have the same color. However, the color pressure energy cannot segment targets with complex colors or textures.

Recent studies have examined external energies based on texture properties since color-based external energies have difficulty dealing with complex textured images. Researchers have shown that by adding new balloon energy based on texture properties to parametric active contour models, it is possible to segment texture objects in the textured background [27].

Vard et al. [33] presented an active contour based on texture properties, which used region information to enhance its ability to capture object boundaries in the image using the texture energy moment equations. Vard et al. [27] also used Walsh Hadamard's transform in another study to obtain region information and obtained better results.

Moallem et al. [28] used the Gabor filter to add image texture information to the active contour. Based on their results, the active contour method which uses a Gabor filter has a better response than the active contour method using a moment.

The above methods are effective for segmenting synthetic images, but they are not accurate enough in order to segment natural images. To overcome this problem, Wu et al. [23] proposed a combination of the Gabor filter and the GLCM algorithm. This combination was used to obtain region information and to construct a new model for a geometric active contour. Due to the GLCM algorithm and geometric active contour, this

method is very slow. By combining local variation degree (LVD) of intensity and Gabor features, Gao et al. [34] added new texture energy to the active contour. Due to the use of a level set contour, this method is very slow, too. Subudhi and Mukhopadhyay [35] presented a statistical region-based Active Contour Model (ACM) that considered the correlation between local and global image statistics to segment cluttered images. Wu et al. [36] proposed Deep Parametric Active Contours (DPAC). Using such high-dimensional features may improve segmentation accuracy, however, calculations of these high-level features burden high computational cost. Subudhi and Mukhopadhyay [16] introduced a new energy using discrete cosine transforms, directing the active contour towards the object boundary. Also Badoual [37] introduced the contour which was directed to the boundary of the target object by including a circle wavelet in the active model.

Due to the high calculation requirements of geometric models [16], the focus of this paper is on active contour models for object segmentation in the textural environment. With the help of the Jensen-Tsallis divergence, new texture properties are added to the parametric active contour model. Jensen-Tsallis divergence (JTD) calculates the distance between two probability density functions, and it is maximal at the boundary between the two probability density functions. If an image consists of two different textures, then the image histogram has two probability density functions, an object probability density function, and a background probability density function. Since the Jensen-Tsallis divergence at the boundary between the two density functions is at a maximum level, if we add it to the active contour, the contour energy equation at the boundary between the target object and the background is minimized.

The structure of this paper is as follows. The mathematical background which contains three parts of ACM, GLCM, and JTD is presented in section 2. In section 3, the proposed method of the active contour model based on JTD is described. The experimental results and validation of the proposed method are discussed in section 4, and the conclusion follows in section 5.

## 2. BACKGROUND

### 2.1. Mathematical Description of the Parametric Active Contour Model

In the parametric active contour model, the contour or surface is specified in parametric form during the deformation process. Parametric active contours are open or closed contours [25], as described in Equation (1):

$$S(u) = I(x(u), y(u)) \quad , \quad u \in [0, 1] \quad (1)$$

The points of the contour move in coordinate space  $(x, y)$  until they match the desired properties of the object. It is necessary to take the vector discrete function  $S(u)$  in the set of points [22] where  $i = 0, 1, \dots, M$ , where  $M$  is the number of points on the contour. In the following, the interpolation of discrete points results in a continuous contour in the final stage. Based on the sum of the two internal energies  $E_{int}(S(u))$  and the external energy  $E_{ext}(S(u))$ , the contour energy  $E(S(u))$  is calculated as follows:

$$E(S(u)) = E_{int}(S(u)) + E_{ext}(S(u)) \quad (2)$$

An effective boundary for segmentation is when the energy from the above equation is the lowest. Thus, finding the boundary of the object will correspond to minimizing the contour energy function. The amount of elasticity and bending of the contour is determined by the internal energy, which is calculated as follows:

$$E_{int} = \frac{\alpha}{2} \left| \frac{\partial}{\partial u} S(u) \right|^2 + \frac{\beta}{2} \left| \frac{\partial^2}{\partial u^2} S(u) \right|^2 \quad (3)$$

Internal energy prevents the points of contour from oscillating and keeps them at a constant distance from one another. The first and second parts of the internal energy respectively prevent excessive elasticity and bending of the contour and keep it cohesive and smooth. In this case, the obtained flexible model will act as a string with both elasticity and strength properties. By adjusting the weighting parameters  $\alpha$  and  $\beta$ , it is possible to adjust the two properties of elasticity and bending concerning each other.

External energy is defined in the scope of the image. It is responsible for absorbing contours into the desired features in an image, such as lines, corners, and other image properties. Therefore, external energy is also known as image energy ( $E_{img}(S(u))$ ). As a result, the parametric active contour energy is defined according to Equation (4):

$$E = \frac{\alpha}{2} \oint \left| \frac{\partial}{\partial u} S(u) \right|^2 du + \frac{\beta}{2} \oint \left| \frac{\partial^2}{\partial u^2} S(u) \right|^2 du + \oint E_{img}(S(u)) du \quad (4)$$

In the traditional model of a parametric active contour, the active contour is deformed enough to capture the actual boundaries of the object to an acceptable extent. For this reason, in the initial active contour models, the image energy was proposed in proportion to the edge characteristic [12, 20]. It was described according to Equation (5) [25] and Equation (6) [38]:

$$E_{img} = E_{edge} = -|\nabla I(s)|^2 \quad (5)$$

$$E_{img} = E_{edge} = -\gamma |\nabla(G_\sigma(s) \times I(s))|^2 \quad (6)$$

Equation (6) is used to reduce noise in which  $\gamma$  is a parameter that controls the amount of image energy.  $\nabla$  is Gradient operator and  $G_\sigma(s) \times I(s)$  shows image

convolution with a Gaussian filter including standard deviation  $\sigma$ .

## 2. 2. Gray-Level Co-Occurrence Matrix

The gray-level co-occurrence matrix is used to extract second-order statistics from an image. The co-occurrence matrix represents the number of times two pixels occur in an image in the direction of a given vector, called the displacement vector. By changing the direction of the vector, we can obtain different characteristics for the texture. The co-occurrence matrix for an image  $I(x, y)$  is defined as Equation (7) [23]:

$$P(x, y) = Pr(x, y|d, \theta, G, W) \quad (7)$$

In the above equation,  $d$  is the distance;  $\theta$  is the direction of movement;  $G$  is the quantization level; and  $W$  is the window size. Once the co-occurrence matrix is formed, various properties can be calculated. In this paper, a new feature is calculated by the Jensen-Tsallis divergence, which is described in the next section.

## 2. 3. Jensen -Tsallis Divergence

Information theory is one of the new scientific branches in applied mathematics and electrical engineering in which information is quantified and studied from a mathematical point of view. Information theory is based on the science of statistics and probability, in which entropy is a fundamental quantity. According to this theory, the concept of entropy is introduced as a branch of image processing that estimates the amount of information in an image. Entropy can provide a sufficient level of image information. Since probabilities are represented by entropy, this is a meaningful measure for texture.

The desired entropy can be calculated from the distribution of the gray level of the image. Since the new external energy is defined based on it, entropy helps the active contour to be better absorbed towards the object boundary. In this case, if each gray level  $r$  occurs with a probability of  $p$ , then the occurring probability of a pixel can be defined as follows:

$$p_k = \frac{n_k}{N \times M} \quad k = 0, \dots, L - 1 \quad (8)$$

$n_k$  indicates the number of pixels on the gray surface  $k$ , and  $L$  represents the number of gray levels.  $M, N$  also represents the number of rows and columns in the image, respectively [39].

## 2. 4. Relative Entropy (Divergence)

Shannon defined entropy for discrete random variables for the first time in 1948 [40]. This entropy is known as Shannon entropy that is described as follows:

$$S(P) = \sum_{k=0}^{L-1} P_k \log(P_k^{-1}) \quad k = 0, 1, 2, \dots, L - 1 \quad (9)$$

Visually, entropy measures the amount of formation or uncertainty in a random variable related to a natural

process. Divergence, also known as relative entropy, is the distance between two probability distribution functions. Divergences have been proposed as a measure of similarity between two probability distribution functions. In information theory, the most important divergence is the Kullback-Leibler (KLD) Divergence between P and Q [41], which is defined as follows:

$$KLD(P \parallel Q) = \sum_{k=0}^{L-1} \log \frac{p_i}{q_i} \quad (10)$$

In classical information theory, this function, known as reciprocal entropy or directional divergence, measures uncertainty in relative rather than absolute terms [42]. The relative entropy is always non-negative and is zero only if  $P = Q$ . However, this is not a real distance between distributions since it is not symmetric and does not satisfy the triangle inequality [43]. When the Kullback-Leibler divergence is zero, we can expect similar (not exactly the same) behavior from two distributions, while a value of 1 indicates that the two distributions have opposite behaviors. A Jensen-Shannon Divergence (JSD) is a finite, symmetric, and smooth version of the Kullback-Leibler Divergence [44], that is defined as follows:

$$JSD(P \parallel Q) = \frac{1}{2}KLD(P \parallel Q) + \frac{1}{2}KLD(Q \parallel M) \quad (11)$$

where  $M = (P + Q) / 2$  in probability information theory and statistics, JSD is a popular method for determining the similarity of two probability distributions. Jensen-Shannon divergence has the following properties: (A) it has mathematical properties and KLD divergence interpretations, and it offers simple interpretations within the framework of statistical physics and information theory; (B) it is symmetrical and works in a metric space; (C) it can be generalized to more than two distributions [45].

Various generalizations of Shannon entropy have been proposed in recent years. The generalization of the Shannon entropy standard is called the Tsallis Entropy as defined below [46]:

$$T^\kappa(P) = \frac{1 - \sum_{k=0}^{L-1} p_k^\kappa}{\kappa - 1} \quad \kappa > 0, \kappa \neq 1 \quad (12)$$

The new form of divergence can be introduced by substituting Tsallis entropy with Shannon entropy in Equation (13). It is known as Jensen-Tsallis divergence and is defined as follows [45]:

$$JTD^\kappa(P, Q) = T^\kappa\left(\frac{P+Q}{2}\right) - \frac{1}{2}[T^\kappa(P) + T^\kappa(Q)] \quad (13)$$

In a picture with a background and a target object, an image histogram diagram shows the image content using two bell-shaped curves (probability density functions), one for the background and the other for the target object. We can separate the pixels related to background and target objects if we can calculate the boundary between these two probability density functions. Different methods have been proposed to obtain the distance

between two probability density functions, such as Kolbeck-Liber, Cauchy-Schwarz, Jensen-Shannon, and Jensen-Tsallis Divergences [47]. This paper shows that the maximum Jensen-Tsallis divergence occurs at the boundary of two density functions, and thus can be recognized as a threshold between target and background objects. Jensen-Tsallis divergence is used by the proposed method to calculate new energy that, when added to Equation (2), will minimize the energy of the active contour exactly at the object boundary. This is described in the following section.

### 3. THE PROPOSED MODEL OF ACTIVE CONTOUR BASED ON JENSEN-TSALLIS DIVERGENCE BALLOON ENERGY

In this paper, a new active contour model based on Jensen-Tsallis divergence is proposed. As described previously, Jensen-Tsallis divergence can be used to determine the boundary between two textures in an image. Since the Jensen-Tsallis divergence is described based on the brightness level of an image, it does not work well in images with inhomogeneous textures. First, the image is described using the co-occurrence matrix algorithm, and then using the Jensen-Tsallis divergence, a new property is extracted from the co-occurrence matrix, which can mention the distinction between two textures in the image. This property is utilized to generate new balloon energy that greatly increases the convergence power of the active parametric contour toward the object boundary.

**3. 1. Balloon Energy Based on Texture** As described in section 1, the active contour model is expressed as Equation (2). The balloon energy based on the texture feature is added to the external energy of the contour equation to increase the strength of the active contour. Therefore, the new external energy is defined by Equation (14):

$$E_{ext} = E_{img} + \lambda \cdot E_{bal} \quad (14)$$

the balloon energy factor  $\lambda$  helps the active contour cross local minima. In the proposed method,  $E_{bal}$  is Equation (15):

$$E_{bal} = -T_{JTD}(I(s)) \times \vec{n}(s) \quad (15)$$

$\vec{n}(s)$  is the unit normal vector of the contour point.

### 3. 2. Algorithm for Segmentation Based on the Proposed Method

The flowchart in Figure 1 illustrates how to segment a textured object in a textured background. The first step is to create the initial contour around the target object in the image. As Equation (4) moves this contour towards the boundary of the target object, an update to Equation (4) is required for a better

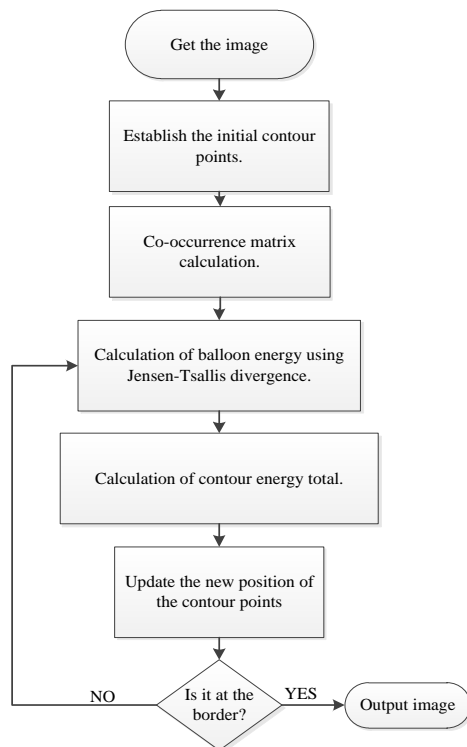


**Figure 1.** The flowchart for the proposed algorithm

active contour function. To achieve this, balloon energy is added to the active contour energy of Equation (4), which improves the active contour's function. The balloon energy is derived from the Jensen-Tsallis divergence. Jensen-Tsallis divergence is calculated by using the texture feature of the image. An image's texture feature can be computed using the GLCM matrix. Therefore, by combining the texture feature and Jensen-Tsallis divergence, novel balloon energy is created. By replacing the existing balloon energy in Equation (4), the total active contour energy equation will be updated. Since the Jensen-Tsallis divergence peaks at the boundary between two texture regions, and the Balloon energy is negative in Equation (15), the total contour equation (Equation (4)) is minimized at that boundary, leading to the active contour stopping.

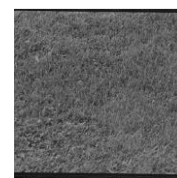
#### 4. EXPERIMENTS AND ANALYSIS OF RESULTS USING VISUAL AND MATHEMATICAL MEASURES

In this section, first under section 4.1, the divergence performance of Jensen-Tsallis is evaluated. According to the experiments, the divergence of Jensen-Tsallis at the boundary between two texture regions is maximum, so the active contour can better determine the boundary between the two regions. In section 4.2, the value of each variable used in the simulations is suggested based on the table. In section 4.3, the proposed method is compared to

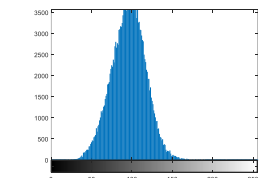
active contour methods based on discrete cosine conversion [16] and active contour methods based on filter bank properties [37]. Simulations are carried out in MATLAB R2016. In the experiments, two groups of images were used. The first group is artificial images from the Brodatz database [48], which consists of two types of textures. The second group is images from the Berkeley database that represent natural images. Images are selected in  $256 \times 256$  sizes.

**4. 1. Jensen-Tsallis Divergence Function** One texture image from Brodatz database is shown in Figure 2. The histogram shows that the gray levels of the image are  $L = 0, \dots, 174$ . A part of another texture is placed inside the previous image to create an image with two textures. As can be seen in the second image, two bell-shaped curves indicate the two textures. As shown in Figure 2, the histogram has been enhanced with gray levels 174 to 221. This means that level 174 is the optimal threshold for detecting boundaries between textures. By applying the Jensen-Tsallis algorithm to the second image, it can be seen that the algorithm is maximized at the level of 168, which can be considered approximating the gray level 168 as the segmentation threshold. Based on the obtained threshold, it can be concluded that the Jensen-Tsallis algorithm can be useful for segmenting such images.

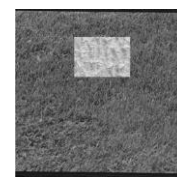
**4. 2. Selecting Parameters** Before performing the tests, six significant parameters need to be adjusted.



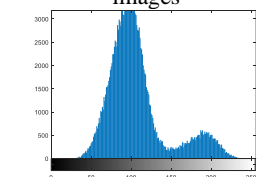
a) Single texture image



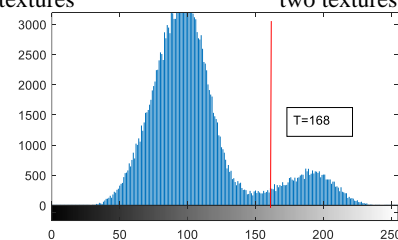
Histogram of single-texture images



b) Image with two textures



A histogram of an image with two textures



C) The result of Jensen-Tsallis divergence

**Figure 2.** Jensen-Tsallis divergence function

First, it examines the  $\alpha$  and  $\beta$  parameters, which are the weights used to calculate the internal energy of a contour. Both the  $\alpha$  and  $\beta$  coefficients are fixed and positive. A value of  $\alpha$  is between  $[0,1]$  and a value of  $\beta$  is between  $[0,0.1]$ . A contour's length and its evolution rate are controlled by the  $\alpha$  parameter, while its curvature is controlled by the  $\beta$  parameter. The active contour jumps over the object boundary if a large value of  $\alpha$  is selected. The active contour becomes very slow and reaches the limit with a significant number of iterations if a value of  $\alpha$  is set too small. In light of other parameters, a value of  $\alpha$  between  $[0.2,0.5]$  is suggested. Generally, the second parameter  $\beta$  is chosen close to 0, otherwise, it might increase contour oscillation, which is undesirable.  $\gamma$  represents the energy factor of the image that helps the active contour move toward the object boundary. This value is chosen between  $[0.01, 0.001]$ . When the active contour faces a local minimization problem, the balloon energy factor  $\lambda$  helps the active contour cross local minima. The value of  $\lambda$  is selected between  $[0,1]$ .  $K$  is the coefficient of the Jensen-Tsallis function for determining the appropriate threshold for separating objects from backgrounds. An amount greater than zero is chosen. LCM is calculated by selecting a window around each pixel image. The size of that window is determined by  $W$ . We should not be too large as it will increase computations and the algorithm will slow down. If  $W$  is selected too small, the texture pattern may not be found. As described in the following Table 1, the above parameters have been used for this paper.

#### 4. 3. Jensen-Tsallis K Parameters Selection

Section 4.1 explains that divergences create a threshold that the active contour can be used to locate the boundary of an object in the image. This paper uses the Jensen-Tsallis divergence for this purpose. A Jensen-Tsallis divergence is a generalized form of Jensen-Shannon divergence that has an adjustment parameter known as  $k$ . When the  $k$ -parameter is changed, a distinct threshold is created that can help the contour move to the boundary of the target object. If  $k = 1$ , the divergence is the same as the Jensen-Shannon divergence, and based on that, the segmentation operation is performed. The best value for  $k$  is chosen based on the images for which Ground Truth is available, along with the flowchart of Figure 3. Initially,  $k_0$  is assumed for the parameter  $k$ , and the new position of the contour in the image is determined based on this assumption. Depending on the position of the contour and how many setpoints of the active contour have reached the boundary, the decision is made to

TABLE 1. Parameters values of the proposed algorithm

$\alpha$	$\beta$	$\gamma$	$\lambda$	$W$
0.2	0.05	0.001	0.2	5

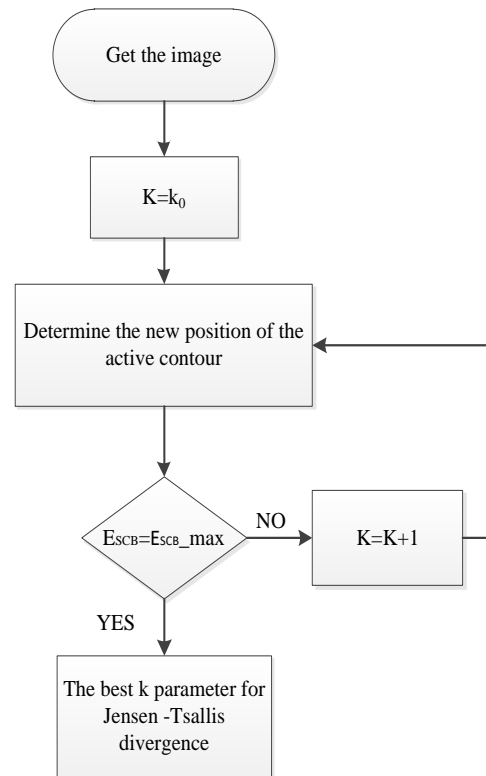


Figure 3. A flowchart for determining the best parameter  $K$  for the Jensen-Tsallis divergence function

update  $K$ , or to complete the process selection of parameter  $K$ . To update parameter  $K$ , it is increased one unit, then the percentage of setpoints that reach the boundary is calculated. This process is repeated until the contour approximates the object boundary or matches it. For updating  $K$ , adding one unit to the value of  $k$ , and calculating the percentage of points touching the boundary is adjusted. This process is repeated until the contour approximates the object boundary or matches it. The value of  $k$  at which the most contour setpoints reach the boundary is used as the divergence parameter ( $k$ ). Next, other images are segmented using the  $K$  selected in the previous step. It is significant to note that the value of  $k$  is between zero and one. The  $k$  parameter in this study is selected by incrementing it by 0.0015 for each iteration and the most accurate value for  $k$  is about 0.08.

#### 4. 4. Test Results

In this section, the proposed method is applied to two groups of images (artificial images and natural images). Figure 4 demonstrates the superiority of Jensen-Tsallis divergence segmentation over other divergences. Figure 5 shows four artificial images with different textures, the first row of which shows the initial contour, and the fourth row shows the segmentation results for each image. In Figure 5, the second and third rows compare segmentation results for methods using discrete cosine conversions [16] and filter

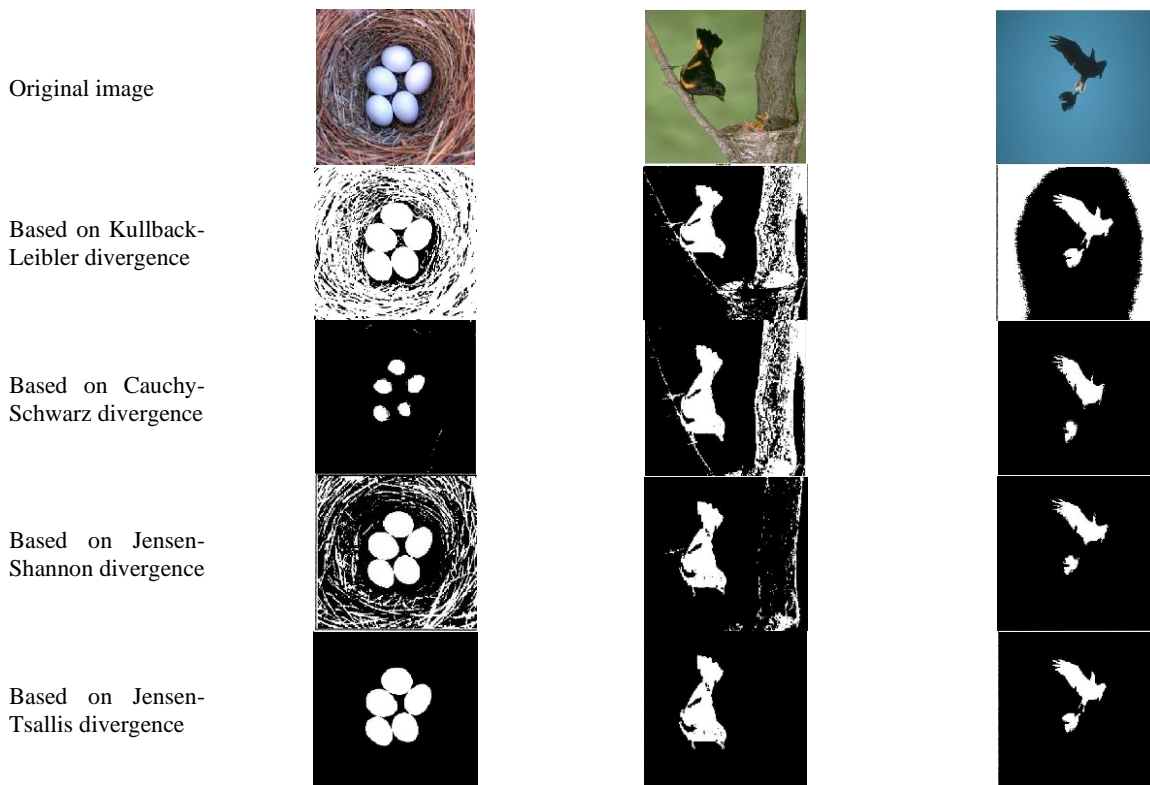


Figure 4. Segmented results of three images using four divergences

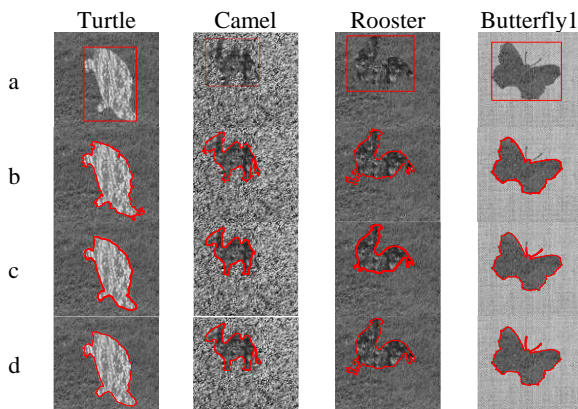


Figure 5. Comparison of segmentation results for synthetic images, a) initial contour, b) based on DCT [16], c) based on filter banks [37], and d) the proposed method

bank texture properties [37]. These simulations visually demonstrate the superiority of the proposed method over other methods. In Figure 6, the simulation results of the proposed method are shown on a variety of natural texture images to analyze its performance further.

#### 4. 5. Performance of Jensen-Tsallis Divergence Compared to Other Divergences

In section 3.2, various methods are described for obtaining the distance between two probability density functions, such as the

Kullback-Leibler, Cauchy-Schwarz, Jensen-Shannon, and Jensen-Tsallis divergences. Distance between two probability density functions is crucial for distinguishing two areas within an image. Equation (13) states that the Jensen-Tsallis divergence function has a variable parameter  $k$ . The variable parameter allows the algorithm to better find the boundary between the two areas of the image and will allow the best segmentation to occur. When  $k$  is 1, the Jensen-Tsallis divergence is the same as the Jensen-Shannon divergence.

#### 4. 6. Quantitative Evaluation

When evaluating the performance of a method, just a visual comparison will not suffice, and the results should be analyzed through various parameters. Two quantitative parameters were used to compare our method with the previous approaches. The first of these is the Maximum Distance of the obtained Active contour from the Desired contour (MDAD) [49], which is defined as follows:

$$MDAD = \max \left( \min \left( d(C(s), \hat{C}) \right) \right) \quad (16)$$

In this equation,  $d(C(s), \hat{C})$  is the distance between the active contour and the desired contour  $C$ . Second,  $E_{SCB}$  [28] is used, whose equation is as follows:

$$E_{SCB} = \frac{SCB(N)}{N} \quad (17)$$

In Equation (17),  $N$  is the number of contour points and  $SCB(N)$  is the number of contour points that fall on the object boundary.

In Table 2, the MDAD values for all of the above images are shown after applying the three methods. In all images, a small amount of MDAD indicates a contour that is closer to the actual contour, which means better segmentation of the subject. In Table 3, a comparison of the  $E_{SCB}$  percentages for all test images is shown. Table 3 shows that, unlike the other two approaches, the proposed method has a higher  $E_{SCB}$  percentage, which means that more contour points are correctly located at the boundary.

**4. 7. Robustness to Noise** To evaluate the noise performance, the proposed method was tested by adding two types of noise to a textured image. In the first experiment, Gaussian noise with zero mean and different variances was applied to the image and the robustness of the proposed method was evaluated. In Figure 7, the first row shows the Gaussian noisy images as well as the segmentation results. The next experiment included Salt and Pepper noise of various densities, added to the image for robustness evaluation.

**TABLE 2.** A comparison between the MDAD parameter in the proposed method and two other methods for segmenting textural images

Test images	Methods		
	DCT energy-based [16]	based on filter banks [37]	Proposed
Turtle	6.4	6.1	5.4
Camel	5.2	4.6	4.2
Rooster	5.0	4.7	4.5
Butterfly1	5.2	5.8	5.1
Tiger	11.2	3.3	3.2
Dog1	10.7	11.0	4
Dog2	9.7	10.1	9.6
Butterfly2	5.1	5.5	4.4

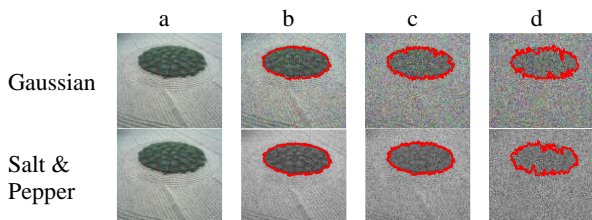


**Figure 7.** The effect of two types of noise on the input image and the segmentation results using the proposed method. Gaussian: a) original image, b)  $\sigma^2 = 0.1$ , c)  $\sigma^2 = 1$ , d)  $\sigma^2 = 1.9$ , Salt & Pepper: a) original image, b)  $d = 0.1$ , c)  $d = 0.5$ , d)  $d = 0.7$

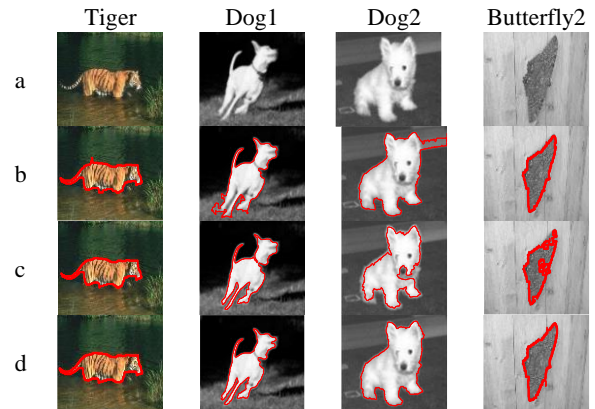


**Figure 6.** Comparison of segmentation results for natural images, a) original image, b) based on DCT [16], c) based on filter banks [37], and d) the proposed method

**TABLE 3.** A comparison between the  $E_{SCB}$  parameter in the proposed method and two other methods for segmenting textural images

Test images	Methods		
	DCT energy-based [16]	based on filter banks [37]	Proposed
Turtle	88.7	90.6	95
Camel	88.6	78.4	95
Rooster	87.3	77.9	94
Butterfly1	75	93.2	94.3
Tiger	91	83.1	93
Dog1	79.3	80.1	96.0
Dog2	75	83.3	87
Butterfly2	90.3	92.2	92

The second row shows noisy images and results of segmentation at noise densities of  $d = 0.1, 0.5$ , and  $0.7$ , where, for example,  $d = 0.1$  means 10% of the pixels in the image are noisy. Based on these experiments, the proposed method is typically able to segment objects correctly even if noise levels are high.

#### 4. 8. Comparison of the Speed of the Proposed Method with other Methods

In this subsection, the time consumed for execution of the proposed algorithm is compared with two previous works. These three methods were tested on textured images with different and complex objects. The test images have  $256 \times 256$  dimensions. For these eight images, Table 4 shows the convergence time of the three methods. According to Table 4, the proposed method takes less time than the other compared methods. Thus, the proposed algorithm is faster for the purpose of detecting textured objects.

**TABLE 4.** Comparing the convergence time of two previous methods and the proposed algorithm

Test images	Methods	Execution time (s)
Turtle	DCT energy-based [16]	44
	based on filter banks [37]	65
	Proposed	35
Camel	DCT energy-based [16]	43
	based on filter banks [37]	62
	Proposed	34
Rooster	DCT energy-based [16]	47
	based on filter banks [37]	64
	Proposed	36
Butterfly1	DCT energy-based [16]	45
	based on filter banks [37]	63
	Proposed	35
Tiger	DCT energy-based [16]	47
	based on filter banks [37]	66
	Proposed	34
Dog1	DCT energy-based [16]	45
	based on filter banks [37]	66
	Proposed	33
Dog2	DCT energy-based [16]	42
	based on filter banks [37]	63
	Proposed	32
Butterfly2	DCT energy-based [16]	43
	based on filter banks [37]	64
	Proposed	33

## 5. CONCLUSION

In this paper, a novel active contour model based on the Jensen-Tsalis divergence is presented that can be applied to artificial texture images as well as natural textures. To improve the active contour performance, the old external energy of the active contour has been combined with the new external energy based on the area information of the image. because information about the area helps the contour to be better absorbed towards the object's edge. The external energy is calculated based on the features extracted from the integration of the co-occurrence matrix method and Jensen-Tsallis divergence, and it corrects the previous external energy. MATLAB software was used to conduct the simulations. Experimental results show that segmentation results are better for both artificial and natural textures.

In addition to converging the contour to the exact

boundary of the object, this method also solves the problem of local minimization. The method uses a parametric active contour, so it is faster than methods that use a level set contour. However, the use of the GLCM algorithm slows down the segmentation process, so it cannot be applied to online applications. The proposed model is limited in segmentation of one object at a time and is not developed for multiple objects simultaneously. This is the main limitation of all parametric active contour models. We plan to implement a new active contour model based on more flexible divergences in the future works.

## 6. REFERENCES

1. Eng, H.-L., Thida, M., Chew, B.-F., Leman, K. and Anggrelly, S.Y., "Model-based detection and segmentation of vehicles for intelligent transportation system", in 2008 3rd IEEE Conference on Industrial Electronics and Applications, IEEE. (2008), 2127-2132. <https://doi.org/10.1109/ICIEA.2008.4582895>
2. Huang, K. and Tan, T., "Vs-star: A visual interpretation system for visual surveillance", *Pattern Recognition Letters*, Vol. 31, No. 14, (2010), 2265-2285, <https://doi.org/10.1016/j.patrec.2010.05.029>.
3. Salimi, A., Pourmina, M.A. and Moin, M.-S., "Fully automatic prostate segmentation in mr images using a new hybrid active contour-based approach", *Signal, Image and Video Processing*, Vol. 12, No. 8, (2018), 1629-1637, doi.
4. Jabbari, S. and Baleghi, Y., "Segmentation of skin lesion images using a combination of texture and color information", *Journal of Soft Computing and Information Technology*, Vol. 8, No. 4, (2020), 87-97, doi.
5. Mahdiraji, S.A., Baleghi, Y. and Sakhaei, S.M., "Skin lesion images classification using new color pigmented boundary descriptors", in 2017 3rd International Conference on Pattern Recognition and Image Analysis (IPRIA), IEEE. (2017), 102-107. <https://doi.org/10.1109/PRIA.2017.7983026>
6. Mahdiraji, S.A., Baleghi, Y. and Sakhaei, S.M., "Bibs, a new descriptor for melanoma/non-melanoma discrimination", in Electrical Engineering (ICEE), Iranian Conference on, IEEE. (2018), 1397-1402. <https://doi.org/10.1109/ICEE.2018.8472701>
7. Chen, Q., Sun, Q.-S., Heng, P.A. and Xia, D.-S., "Two-stage object tracking method based on kernel and active contour", *IEEE Transactions on Circuits and Systems for Video Technology*, Vol. 20, No. 4, (2010), 605-609, <https://doi.org/10.1109/TCSVT.2010.2041819>.
8. Nikbakhsh, N., Baleghi, Y. and Agahi, H., "Maximum mutual information and tsallis entropy for unsupervised segmentation of tree leaves in natural scenes", *Computers and electronics in Agriculture*, Vol. 162, (2019), 440-449, <https://doi.org/10.1016/j.compag.2019.04.038>.
9. Nikbakhsh, N., Baleghi, Y. and Agahi, H., "A novel approach for unsupervised image segmentation fusion of plant leaves based on g-mutual information", *Machine Vision and Applications*, Vol. 32, No. 1, (2021), 1-12.
10. Nikbakhsh, N., Baleghi Damavandi, Y. and Agahi, H., "Plant classification in images of natural scenes using segmentations fusion", *International Journal of Engineering*, Vol. 33, No. 9, (2020), 1743-1750.
11. Asvadi, A., Mahdavinataj, H., KARAMI, M.R. and Baleghi, Y., "Online visual object tracking using incremental discriminative

- color learning", *The CSI Journal on Computer Science and Engineering*, Vol. 12, No. 24, (2014), 16-28, doi.
12. Asvadi, A., Karami-Mollaie, M., Baleghi, Y. and Seyyedi-Andi, H., "Improved object tracking using radial basis function neural networks", in 2011 7th Iranian Conference on Machine Vision and Image Processing, IEEE. (2011), 1-5. <https://doi.org/10.1109/IranianMVIP.2011.6121604>
  13. Asvadi, A., Karami, M. and Baleghi, Y., "Efficient object tracking using optimized k-means segmentation and radial basis function neural networks", *International Journal of Information and Communication Technology Research*, Vol. 4, No. 1, (2012), 29-39, doi.
  14. Asvadi, A., Karami, M. and Baleghi, Y., "Object tracking using adaptive object color modeling", in Proceeding of 4th Conference on Information and Knowledge Technology. (2012), 848-852.
  15. Asvadi, A., Mahdavinataj, H., Karami, M. and Baleghi, Y., "Incremental discriminative color object tracking", in International Symposium on Artificial Intelligence and Signal Processing, Springer. (2013), 71-81.
  16. Subudhi, P. and Mukhopadhyay, S., "A fast texture segmentation scheme based on active contours and discrete cosine transform", *Computers & Electrical Engineering*, Vol. 62, (2017), 105-118, <https://doi.org/10.1016/j.compeleceng.2017.04.021>.
  17. Sagiv, C., Sochen, N.A. and Zeevi, Y.Y., "Integrated active contours for texture segmentation", *IEEE Transactions on Image Processing*, Vol. 15, No. 6, (2006), 1633-1646, <https://doi.org/10.1109/TIP.2006.871133>.
  18. Abdelsamea, M.M., Gnecco, G. and Gaber, M.M., "An efficient self-organizing active contour model for image segmentation", *Neurocomputing*, Vol. 149, (2015), 820-835, <https://doi.org/10.1016/j.neucom.2014.07.052>.
  19. Shantkumari, M. and Uma, S., "Grape leaf segmentation for disease identification through adaptive snake algorithm model", *Multimedia Tools and Applications*, Vol. 80, No. 6, (2021), 8861-8879.
  20. Fu, X., Fang, B., Zhou, M. and Li, J., "Hybrid active contour driven by double-weighted signed pressure force for image segmentation", in ICASSP 2020-2020 IEEE International Conference on Acoustics, Speech and Signal Processing (ICASSP), IEEE. (2020), 2463-2467. <https://doi.org/10.1109/ICASSP40776.2020.9054627>
  21. Cremers, D., Rousson, M. and Deriche, R., "A review of statistical approaches to level set segmentation: Integrating color, texture, motion and shape", *International Journal of Computer Vision*, Vol. 72, No. 2, (2007), 195-215, doi.
  22. Wang, Y. and Zeng, R., "Image segmentation algorithm based on geometric flow bandelets transformation particle replanting", *Pattern Recognition Letters*, Vol. 116, (2018), 200-204, <https://doi.org/10.1016/j.patrec.2018.10.021>.
  23. Wu, Q., Gan, Y., Lin, B., Zhang, Q. and Chang, H., "An active contour model based on fused texture features for image segmentation", *Neurocomputing*, Vol. 151, (2015), 1133-1141, <https://doi.org/10.1016/j.neucom.2014.04.085>.
  24. Caselles, V., Kimmel, R. and Sapiro, G., "Geodesic active contours", *International Journal of Computer Vision*, Vol. 22, No. 1, (1997), 61-79, doi.
  25. Kass, M., Witkin, A. and Terzopoulos, D., "Snakes: Active contour models", *International Journal of Computer Vision*, Vol. 1, No. 4, (1988), 321-331, doi.
  26. Nisirat, M.A., "A new external force for snake algorithm based on energy diffusion", *International Journal of Machine Learning and Computing*, Vol. 9, (2019), 316-321.
  27. Vard, A., Monadjemi, A., Jamshidi, K. and Movahhedinia, N., "Fast texture energy based image segmentation using directional walsh-hadamard transform and parametric active contour models", *Expert Systems with Applications*, Vol. 38, No. 9, (2011), 11722-11729, <https://doi.org/10.1016/j.eswa.2011.03.058>.
  28. Moallem, P., Tahvilian, H. and Monadjemi, S.A., "Parametric active contour model using gabor balloon energy for texture segmentation", *Signal, Image and Video Processing*, Vol. 10, No. 2, (2016), 351-358, doi.
  29. Bae, H.-J. and Jung, S.-H., "Image retrieval using texture based on dct", in Proceedings of ICICS, 1997 International Conference on Information, Communications and Signal Processing. Theme: Trends in Information Systems Engineering and Wireless Multimedia Communications (Cat., IEEE. Vol. 2, (1997), 1065-1068.
  30. Ivins, J. and Porrill, J., "Active region models for segmenting medical images", in Proceedings of 1st International Conference on Image Processing, IEEE. Vol. 2, (1994), 227-231.
  31. Schaub, H. and Smith, C.E., "Color snakes for dynamic lighting conditions on mobile manipulation platforms", in Proceedings 2003 IEEE/RSJ International Conference on Intelligent Robots and Systems (IROS 2003)(Cat. No. 03CH37453), IEEE. Vol. 2, (2003), 1272-1277.
  32. Hamarneh, G., Chodorowski, A. and Gustavsson, T., "Active contour models: Application to oral lesion detection in color images", in Smc 2000 conference proceedings. 2000 ieee international conference on systems, man and cybernetics. cybernetics evolving to systems, humans, organizations, and their complex interactions'(cat. no. 0, IEEE. Vol. 4, (2000), 2458-2463.
  33. Vard, A.R., Moallem, P. and Nilchi, A.R.N., "Texture-based parametric active contour for target detection and tracking", *International Journal of Imaging Systems and Technology*, Vol. 19, No. 3, (2009), 187-198, <https://doi.org/10.1002/ima.20194>.
  34. Gao, M., Chen, H., Zheng, S. and Fang, B., "Feature fusion and non-negative matrix factorization based active contours for texture segmentation", *Signal Processing*, Vol. 159, (2019), 104-118, <https://doi.org/10.1016/j.sigpro.2019.01.021>.
  35. Subudhi, P. and Mukhopadhyay, S., "A statistical active contour model for interactive clutter image segmentation using graph cut optimization", *Signal Processing*, Vol. 184, (2021), 108056, <https://doi.org/10.1016/j.sigpro.2021.108056>.
  36. Wu, X., Tan, G., Li, K., Li, S., Wen, H., Zhu, X. and Cai, W., "Deep parametric active contour model for neurofibromatosis segmentation", *Future Generation Computer Systems*, Vol. 112, (2020), 58-66, <https://doi.org/10.1016/j.future.2020.05.001>.
  37. Badoual, A., Unser, M. and Depeursinge, A., "Texture-driven parametric snakes for semi-automatic image segmentation", *Computer Vision and Image Understanding*, Vol. 188, (2019), 102793, doi: 10.1016/j.cviu.2019.102793.
  38. Prince, J.L. and Xu, C., "A new external force model for snakes", in Proc. 1996 Image and Multidimensional Signal Processing Workshop, Citeseer. Vol. 3, No. 31, (1996), 1.
  39. Mehri, A., Jamaati, M. and Mehri, H., "Word ranking in a single document by jensen-shannon divergence", *Physics Letters A*, Vol. 379, No. 28-29, (2015), 1627-1632, <https://doi.org/10.1016/j.physleta.2015.04.030>.
  40. Shannon, C.E., "A mathematical theory of communication", *The Bell System Technical Journal*, Vol. 27, No. 3, (1948), 379-423.
  41. Mezard, M. and Montanari, A., "Information, physics, and computation, Oxford University Press, (2009).
  42. Klir, G., "Uncertainty and information: Foundation of generalized information theory: John wiley and sons, new jersey", (2006).
  43. Kieffer, J., "Elements of information theory (thomas m. Cover and joy a. Thomas)", *SIAM Review*, Vol. 36, No. 3, (1994), 509-511.

44. Endres, D.M. and Schindelin, J.E., "A new metric for probability distributions", *IEEE Transactions on Information Theory*, Vol. 49, No. 7, (2003), 1858-1860, <https://doi.org/10.1109/TIT.2003.813506>.
45. Angulo, J., Antolín, J., López-Rosa, S. and Esquivel, R., "Jensen–tsallis divergence and atomic dissimilarity for ionized systems in conjugated spaces", *Physica A: Statistical Mechanics and its Applications*, Vol. 390, No. 4, (2011), 769-780, <https://doi.org/10.1016/j.physa.2010.11.005>.
46. Rajinikanth, V., Dey, N., Satapathy, S.C. and Ashour, A.S., "An approach to examine magnetic resonance angiography based on tsallis entropy and deformable snake model", *Future Generation Computer Systems*, Vol. 85, (2018), 160-172, <https://doi.org/10.1016/j.future.2018.03.025>.
47. Baleghi, Y. and Rousseau, D., "An analytical proof on suitability of cauchy-schwarz divergence as the aggregation criterion in region growing algorithm", *Image and Vision Computing*, Vol. 115, (2021), 104312, <https://doi.org/10.1016/j.imavis.2021.104312>.
48. Hersey, I., "Textures: A photographic album for artists and designers by phil brodatz", *Leonardo*, Vol. 1, No. 1, (1968), 91-92.
49. Subudhi, P. and Mukhopadhyay, S., "A pyramidal approach to active contours implementation for 2d gray scale image segmentation", in 2016 International Conference on Wireless Communications, Signal Processing and Networking (WiSPNET), IEEE., (2016), 752-757.

---

### Persian Abstract

---

#### چکیده

بخش بندی تصاویر بافتی، نقش مهمی در عملیات مختلف بینایی ماشین ایفا می کند. مدل های کانتور فعال یکی از کارآمدترین و محبوب ترین روش ها برای شناسایی هدف و بخش بندی اشیا در تصویر هستند. این مقاله یک مدل کانتور فعال پارامتری (PACM) با یک چارچوب کمینه سازی مقاوم بر اساس انرژی بافت تصویر ارائه می کند. ابتدا، ویژگی های بافت تصویر اصلی با استفاده از GLCM (ماتریس هم رخدادی سطح خاکستری) استخراج می شوند. پس از آن، بر اساس ویژگی های بافت GLCM در داخل و خارج از کانتور فعال، واگرایی جنسن-تسالیس انرژی ها محاسبه می شود. واگرایی جنسن-تسالیس با استفاده از معادله بالون به کانتور فعال پارامتریک اضافه می شود. واگرایی در مرز بین پیش زمینه و پس زمینه تصویر حداکثر است، که منجر به به حداقل رساندن معادله کانتور فعال در مرز جسم هدف می شود. این تابع انرژی کمینه سازی با ویژگی بافت می تواند از وجود حداقل های محلی در مدل های PACM جلوگیری کند. همچنین، برخلاف مدل های قبلی، مدل پیشنهادی فقط به کانتور اولیه نیاز دارد و به فاصله کانتور اولیه از شی هدف وابسته نیست. از نظر دقت و کارایی بخش بندی، آزمایش ها با تصاویر مصنوعی و طبیعی نشان می دهند که رویکرد پیشنهادی نتایج رضایت بخش تری نسبت به روش های اخیر به دست آورده است.

---